(2)

OFFICE OF NAVAL RESEARCH

Contract N00014-82K-0612

Task No. NR 627-838

TECHNICAL REPORT NO. 39

Photophysics and Photochemistry of Tris (2,2'-Bipyridyl) Ruthenium(II) Within The Layered Inorganic Solid Zirconium Phosphate Sulfophenylphosphonate

by

Jorge L. Colon, Chao-Yeuh Yang, Abraham Clearfield
And Charles R. Martin

Prepared for publication

in

The Journal of Physical Chemistry

Department of Chemistry
Texas A&M University
College Station, TX 77843

October 9, 1989

REPORT DOCUMENTATION PAGE

Form Approved
OMB No. 0704-0188

1a. REPORT SECURITY CLASSIFICATION
UNCLASSIFIED

1b. RESTRICTIVE MARKINGS

2a. SECURITY CLASSIFICATION AUTHORITY

2b. DECLASSIFICATION / DOWNGRADING SCHEDULE

3. DISTRIBUTION / AVAILABILITY OF REPORT
Approved for public distribution, distribution unlimited

4. PERFORMING ORGANIZATION REPORT NUMBER(S)
ONR TECH REPORT # 39

5. MONITORING ORGANIZATION REPORT NUMBER(S)

6a. NAME OF PERFORMING ORGANIZATION
C.R. MARTIN
Department of Chemistry

6b. OFFICE SYMBOL (If applicable)

7a. NAME OF MONITORING ORGANIZATION
Office of Naval Research

6c. ADDRESS (City, State, and ZIP Code)
Texas A&M University
College Station, TX77843-3255

7b. ADDRESS (City, State, and ZIP Code)
800 North Quincy Street
Arlington, VA 22217

8a. NAME OF FUNDING / SPONSORING ORGANIZATION
Office of Naval Research

8b. OFFICE SYMBOL (If applicable)

9. PROCUREMENT INSTRUMENT IDENTIFICATION NUMBER
Contract # N00014-82K-0612

8c. ADDRESS (City, State, and ZIP Code)
800 North Quincy Street
Arlington, VA 22217

10. SOURCE OF FUNDING NUMBERS

PROGRAM ELEMENT NO.	PROJECT NO.	TASK NO	WORK UNIT ACCESSION NO

11. TITLE (Include Security Classification)
Phytophysics and Photochemistry of Tris(2,2'-Bipyridyl) Ruthenium(II) Within The Layered Inorganic Solid Zirconium Phosphate Sulfophenylphosphonate (Unclassified)

12. PERSONAL AUTHOR(S)
Jorge L. Colon, Chao-Yeuh Yang, Abraham Clearfield, and Charles R. Martin

13a. TYPE OF REPORT	13b. TIME COVERED	14. DATE OF REPORT (Year, Month, Day)	15. PAGE COUNT
Technical	FROM _____ TO _____	(89,10,09)Oct. 9, 1989	

16. SUPPLEMENTARY NOTATION

17. COSATI CODES		
FIELD	GROUP	SUB-GROUP

18. SUBJECT TERMS (Continue on reverse if necessary and identify by block number)
Photophysics, Photochemistry, Tris(2,2'-Bipyridyl) Ruthenium(II), Zirconium, Phosphate, Sulfophenylphosphonate

19. ABSTRACT (Continue on reverse if necessary and identify by block number)

The photophysics and photochemistry of tris(2,2'-bipyridyl) ruthenium(II) ($Ru(bpy)_3^{2+}$) absorbed into the layered solid zirconium phosphate sulfophenylphosphonate are described. The decay kinetics of the metal complex are shown to depart from first-order behavior. Albery's model of despersed kinetics, which assumes a continuous distribution of rate constants, is used to explain the decay kinetics. The oxidative quencher methylviologen (MV^{2+}) is shown to react with $Ru(bpy)_3^{2+}$ in ZrPS via a combined dynamic and quasi static (sphere of action) quenching mechanism.

20. DISTRIBUTION / AVAILABILITY OF ABSTRACT
☒ UNCLASSIFIED/UNLIMITED ☐ SAME AS RPT ☐ DTIC USERS

21. ABSTRACT SECURITY CLASSIFICATION
Unclassified

22a. NAME OF RESPONSIBLE INDIVIDUAL	22b. TELEPHONE (Include Area Code)	22c. OFFICE SYMBOL
Dr. Robert Nowak	(202)696-4410	

ONR Tech Report #37

PHOTOPHYSICS AND PHOTOCHEMISTRY OF TRIS(2,2'-BIPYRIDYL) RUTHENIUM(II) WITHIN THE LAYERED INORGANIC SOLID ZIRCONIUM PHOSPHATE SULFOPHENYLPHOSPHONATE

JORGE L. COLON, CHAO-YEUH YANG, ABRAHAM CLEARFIELD*, AND CHARLES R. MARTIN*

DEPARTMENT OF CHEMISTRY

TEXAS A&M UNIVERSITY

COLLEGE STATION, TEXAS 77843

* To whom correspondence should be addressed.

ABSTRACT

The photophysics and photochemistry of tris(2,2'-bipyridyl) ruthenium(II) ($Ru(bpy)_3^{2+}$) adsorbed into the layered solid zirconium phosphate sulfophenylphosphonate are described. The decay kinetics of the metal complex are shown to depart from first-order behavior. Albery's model of dispersed kinetics, which assumes a continuous distribution of rate constants, is used to explain the decay kinetics. The oxidative quencher methylviologen (MV^{2+}) is shown to react with $Ru(bpy)_3^{2+}$ in ZrPS via a combined dynamic and quasi static (sphere of action) quenching mechanism.

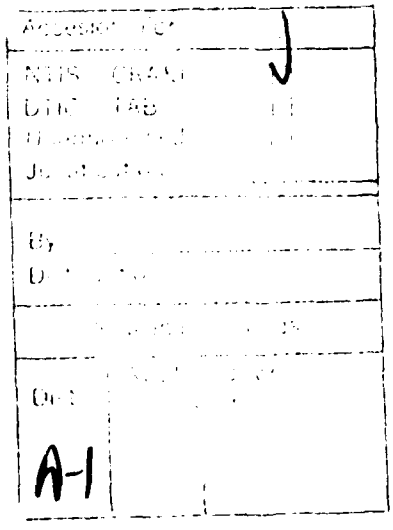

INTRODUCTION

Much of the effort in solar energy research has focused on the use of electron transfer reactions to convert and store solar energy. To meet this goal the energy-releasing back reaction has to be suppressed.[1-3] Recently, several strategies for suppressing the back reaction and enhancing the charge separation efficiency have been devised.[1-3] These new strategies make use of interfaces, surfaces, micelles, polyelectrolytes, and other heterogeneous microenvironments to obtain efficient charge separation.

The layered zirconium phosphates[4] are heterogeneous systems which could prove useful as media for solar energy conversion. Zirconium phosphates are acidic, inorganic, ion-exchange materials having a layered structure.[4] These materials have potential applications as catalysts, ion-exchangers, solid electrolytes, and hosts for various intercalants.[5-7] Organic derivatives of α-zirconium phosphate (α-ZrP, which has the formula $Zr(HPO_4)_2 \cdot H_2O$), have recently been synthesized. These new layered compounds usually have increased interlayer space, reactivity, and selectivity, relative to α-ZrP.[8-15]

We have recently reported preliminary results of characterizations of one of these organic derivatives of α-ZrP, zirconium phosphate sulfophenylphosphonate (ZrPS).[16] In those studies the luminescence probe ion tris(2,2'-bipyridyl) ruthenium(II) ($Ru(bpy)_3^{2+}$) was used to obtain information about the microenvironment within this layered solid.

We have recently investigated excited state reactions between $Ru(bpy)_3^{2+}$ and the quencher methylviologen (MV^{2+}) within ZrPS. We have found that the layered structure of ZrPS affects the lifetime of the excited state of $Ru(bpy)_3^{2+}$. Albery's model for dispersed kinetics in heterogeneous systems[17] was used to describe the $Ru(bpy)_3^{2+}$ decay kinetics in ZrPS. We have also found that the excited state quenching reaction of $Ru(bpy)_3^{2+}$ with MV^{2+} in this system occurs via a combination of diffusional (dynamic/collisional) and sphere of action quenching. The results of these investigations are reported here.

EXPERIMENTAL SECTION

Materials. $Ru(bpy)_3Cl_2 \cdot 6H_2O$ was obtained from G. F. Smith and used as received. 1,1'-dimethyl-4,4'-bipyridinium dichloride hydrate (the cation is called methylviologen, MV^{2+}) was obtained from Aldrich and used as received. Water was either triply distilled or circulated through a Milli-Q water purification system (Millipore Corp.). All other reagents and solvents were of the highest grade available and were used without further purification.

Procedures. The ZrPS, $Zr(HPO_4)(O_3P\text{-}C_6H_4SO_3H)$, was prepared as described previously.[18] $Ru(bpy)_3^{2+}$ was incorporated (loaded) into ZrPS as described in our earlier study.[16] A typical procedure was as follows: Fifty mg of the ZrPS were suspended in water; six mL of a 6.7×10^{-4} M aqueous solution of $Ru(bpy)_3^{2+}$ were added, and the mixture was shaken. Forty μL of this mixture were then used to coat a quartz slide (Esco Products) and the solvent was

allowed to evaporate overnight at room temperature.

This procedure produced a thin (ca. 1.0 μm) film of $Ru(bpy)_3^{2+}$-loaded ZrPS coated onto the quartz slide. The equilibrium water content of these films was ca. 5% by weight (100 X wt of H_2O/wt of dry film). The $Ru(bpy)_3^{2+}$ content was varied by varying the quantity of $Ru(bpy)_3^{2+}$ added to the suspension. ZrPS films containing both $Ru(bpy)_3^{2+}$ and MV^{2+} were obtained by adding measured amounts of both cations to the ZrPS suspension. In the quenching experiments, 2% of the ionic sites in the ZrPS were loaded with $Ru(bpy)_3^{2+}$. This low level of loading was used to insure that no self-quenching of the probe molecules occurred during these experiments. In this way, any observed quenching is the result of interactions between the probe and the quencher ions.

Instrumentation. Steady-state emission spectra were obtained with a Spex Fluorolog 2 spectrofluorometer. The samples were excited with a 450-W xenon lamp. The excitation wavelength was 452 nm. The excitation and emission slits were set at 1.25 mm, yielding a monochromator bandwidth of 4.6 nm. Luminescence was detected perpendicular to the incident radiation with a Hamamatsu R928 photomultiplier tube which was configured for photon counting. The Spex solid sample holder (front-face viewing geometry) was used. A Spex Datamate digitized and displayed the emission data. Electronic absorption spectra were recorded on a Perkin-Elmer Lambda 4B spectrophotometer. X-ray powder diffraction patterns were obtained with a Seifert-Scintag

automated powder diffractometer (PAD II) with a Ni-filtered Cu Kα radiation (λ = 1.5418 Å).

Luminescence lifetimes measurements were obtained by using time-correlated single photon counting (TCSPC)[19,20] on an Edinburgh Instruments Model 199 fluorescence lifetime spectrometer. The excitation source was the 337 nm line of a coaxial thyratron-gated N_2 flashlamp (Edinburgh Instruments model 199F) (< 2 ns full width at half maximum, fwhm). The emission transients were measured at 610 nm. The emitted luminescence was passed through a Schott 3-67 filter before being detected by a Philips XP2254B red-sensitive photomultiplier tube. The pulse repetition rate was 40 kHz and the emission count rate was maintained below 850 Hz to ensure no pulse pileup errors. On the time scale of the decay (> 100 ns) the excitation pulse width (fwhm < 2ns) is negligibly narrow. Therefore, deconvolution of the decay transients was not necessary.

The samples were positioned in the spectrometer at 45 degrees to the axis of excitation. Emission was detected from the opposite side of the film/quartz sample at 45 degrees to the axis of the detector photomultiplier. This orientation (and the emission filter) minimizes the detection of any scattering from the films.

DATA ANALYSES. Data analyses were performed on an IBM PS/2 Model 30 microcomputer with an 8087 math coprocessor. The general approach for obtaining kinetic data from the experimental intensity vs. time transients involved fitting simulated and

experimental transients. Kinetic data were extracted from the best-fit simulated transients. The best fits were determined by the method of nonlinear least-squares (Marquardt algorithm);[19-21] the Edinburgh Instrument's or MTR Software Inc's nonlinear least-squares software was used. The Marquardt algorithm minimizes the goodness-of-fit parameter χ^2 given by:

$$\chi^2 = \Sigma \{ 1/\sigma_i^2 [y_i - y(t_i)]^2 \} \quad (1)$$

where σ_i are the uncertainties (errors) in the data points y_i, and $y(t_i)$ is the value of the fitting function at each data point. For single photon counting data $\sigma_i^2 = y_i$[19-21].

The luminescence of molecules emitting from heterogeneous systems such as proteins, surfaces, micelles, etc., frequently depart form first-order kinetics. Thus, a plot of the logarithm of emission intensity vs. time is nonlinear. In kinetic studies of these systems the nonlinear semilogarithmic plot is usually fitted to a multiexponential decay model. For the studies reported here, three different models were used to calculate the simulated transients. The first was a simple monoexponential decay law:

$$I = B_1 \exp(-k_1 t) \quad (2)$$

where I is the intensity of emission at any time, B_1 is a pre-exponential factor, and k_1 is the decay rate constant.

A double exponential decay expression was also used to fit the data:

$$I = B_1\exp(-k_1t) + B_2\exp(-k_2t) \quad (3)$$

where B_1 and B_2 are pre-exponential factors, and k_1 and k_2 are decay rate constants. This model assumes that there are two populations of emitters, one which decays with a rate constant k_1 and another which emits with a rate constant k_2. The relative numbers of emitters in each population are given by the fractions B_1 and B_2 ($[B_1/(B_1 + B_2)] + [B_2/(B_1 + B_2)] = 1$).

The third model used to fit our data was an adaptation of a new model for interpreting the decay kinetics in nonhomogeneous systems. Rather than assuming just one or two distinct populations of emitters, this model assumes that a continuous distribution of decay rates exist within the heterogeneous system. This continuous distribution of decay rates results from a continuous distribution of chemical microenvironments within the system; thus, each microenvironment has a distinct decay rate constant. This model assumes that each of these rate constants is first-order.

Several research groups have tried to extract the specific distribution of the rate constants from the decay data, a difficult task given the complexity of these systems. Ware et al.,[22-25] Lakowicz et al.,[26-28] and Gratton et al.,[29-32] have simplified this task by assuming a Gaussian or Lorentzian distribution of the lifetimes.

Recently , Albery et al.[17] proposed a general model for dispersed kinetics in heterogeneous systems. This model assumes that the dispersion in the kinetics is the result of a change in energy of activation for the reaction at different sites in the system. Albery's model assumes that the observed kinetics can be described by a Gaussian distribution of the energies of activation or of the natural logarithm of the decay rate constant.

We have used Albery's dispersed kinetics model as the third approach for fitting experimental emission decay curves. The equation used to fit the decay curves to this Gaussian distribution model is:[17]

$$C/C_o = \frac{\int_{-\infty}^{+\infty} \exp(-x^2)\ \exp[-\tau\ \exp(\gamma x)]\ dx}{\int_{-\infty}^{+\infty} \exp(-x^2)\ dx} \qquad (4)$$

where

$$\int_{-\infty}^{+\infty} \exp(-x^2)\ dx = \pi^{1/2}$$

C is the concentration of excited state species at any time t after excitation, C_o is the excited state concentration at t = 0, x is the parameter that describes the Gaussian, γ corresponds to the width of the distribution, and $\tau = \bar{k}t$. The decay rate constant of maximum probability is $\bar{k}$. The τ in Equation 4 should not be confused with the average lifetime for the emitter which is $1/\bar{k}$. Details of this analysis can be found in reference 17.

A detailed derivation of Equation 4 is provided in reference 33.

RESULTS AND DISCUSSION

Self-Quenching Studies. Figure 1 shows typical luminescence decay curves for $Ru(bpy)_3^{2+}$ exchanged into ZrPS at various loading levels. In general the decay becomes faster as the amount of $Ru(bpy)_3^{2+}$ loaded increases. Note that the data are plotted in semilogarithmic fashion in Figure 1; the nonlinearity indicates that a simple monoexponential decay model (Equation 2) will not fit the data. Nonexponential decay is typically observed for luminescent molecules emitting from heterogeneous systems. For example, Turro et al. observed nonexponential decay for $Ru(bpy)_3^{2+}$ adsorbed within a layered solid.[34]

Figure 2 shows typical fits of the experimental luminescence decay data for $Ru(bpy)_3^{2+}$ in ZrPS to Albery's dispersed kinetics model (Equation 4) and the biexponential decay model (Equation 3). The kinetic and statistical parameters associated with the best fit of the biexponential decay model to the experimental data are presented in Table I. The kinetic and statistical parameters associated with the best fit of Albery's dispersed kinetics model to the experimental data are presented in Table II. The χ^2 values for the biexponential decay model are essentially identical to the χ^2 values for the dispersed kinetics model. However, whereas the biexponential decay model has three adjustable parameters (two decay rates and one pre-exponential), the dispersed kinetics model has only two adjustable parameters ($\bar{k}$, the average decay rate constant, and γ, the width of the

distribution). The principle of "Ockham's razor"[35] makes the dispersed kinetics model preferable to the biexponential model.

More important than the "Ockham's razor" argument, the standard deviations of the parameters obtained from the fit to the dispersed kinetics model were always 3 to 10 times smaller than for the biexponential fit (Tables I and II). The smaller standard deviations provide quantitative statistical evidence that the dispersed kinetics model provides a better fit to the experimental data.

The ability of the Albery dispersed kinetics model to fit the luminescence decay data suggests that a multiplicity of binding sites are present in ZrPS. This multiplicity of chemical microenvironments produces slightly different photophysics for the $Ru(bpy)_3^{2+}$ ions residing within these distinct microenvironments. As a result, a continuous distribution of decay rate constants is obtained.[33]

The existence of a variety of microenvironments in ZrPS results from the heterogeneous structure of ZrPS. The stoichiometry of ZrPS would suggest that the sulfonated phenylphosphonate groups are separated by the P-OH group on an adjacent phosphate group. However, ZrPS is a random, rather than an alternating, copolymer. Thus, there is a multiplicity of distances between the phenylphosphonate groups which creates a multiplicity of chemical microenvironments in which the luminescence probe can reside. This heterogeneity of the microenvironment in ZrPS, both within the two dimensional

structure of each layer and between adjacent layers, is responsible for the observed dispersion in the $Ru(bpy)_3^{2+}$ luminescence decay kinetics.

A plot of mean excited state lifetime (obtained by fitting the data to the dispersed kinetics model) vs. quantity of $Ru(bpy)_3^{2+}$ exchanged into ZrPS is shown in Figure 3. Note first that the lifetime at low loading levels is longer than the lifetime for $Ru(bpy)_3^{2+}$ in either aerated or deaerated aqueous solution (434 and 600 ns, respectively). Ghosh and Bard observed similarly protracted excited state lifetimes for $Ru(bpy)_3^{2+}$ confined to a hectorite clay.[36]

Our previous X-ray diffraction studies indicated that $Ru(bpy)_3^{2+}$ resides in the interlayer space of ZrPS.[16] The protracted excited state lifetime for $Ru(bpy)_3^{2+}$ results from the rigid microenvironment within this interlayer space. This rigid microenvironment impedes vibrational deactivation of the excited state. Furthermore, the extent of charge transfer to solvent (water) may also be diminished in the interlayer space.

Figure 3 also shows that the mean luminescence lifetime decreases as the concentration of $Ru(bpy)_3^{2+}$ exchanged into the ZrPS films increases. This decrease in luminescence lifetime clearly indicates that self-quenching is occurring in the ZrPS films. Furthermore, Figure 1 indicates that the quenching process occurs via a dynamic mechanism since the luminescence intensities at t=0 are all the same. Stern-Volmer analysis

allows for a quantitative description of the dynamic quenching process[37,38]

$$\tau_o/\tau = 1 + k_q\tau_o[Ru(bpy)_3^{2+}] \quad (5)$$

$$1/\tau = 1/\tau_o + k_q[Ru(bpy)_3^{2+}] \quad (6)$$

$$k = k_o + k_q[Ru(bpy)_3^{2+}] \quad (7)$$

where τ_o is the lifetime of the probe without quencher, τ is the lifetime of the probe with added quencher, k_q is the bimolecular quenching rate constant, k is the decay rate, and k_o is the decay rate constant of the probe in the absence of quencher. Figure 4 shows a Stern-Volmer (Equation 7) plot of the data from Figure 3; as predicted by Equation 7, this plot is linear (R=0.999). This indicates that a dynamic mechanism is responsible for the self-quenching process. The slope of this line yields a self-quenching rate constant of 7.0×10^5 M^{-1} s^{-1}.

Similar results for the $Ru(bpy)_3^{2+}$ self-quenching reaction have been observed by Milosavljevic and Thomas for $Ru(bpy)_3^{2+}$ confined within a cellulose film;[39] a self-quenching rate constant in cellulose of 7.8×10^6 $M^{-1}s^{-1}$ was obtained. Milosavljevic and Thomas also obtained a $Ru(bpy)_3^{2+}$ self-quenching rate constant of 5.1×10^7 $M^{-1}s^{-1}$ in aqueous solution. A comparison of the magnitudes of the self-quenching rate constants in these three media indicate that diffusion charge transport is more hindered in ZrPS. We address this point in further detail below.

It is of interest to elucidate the mechanism for $Ru(bpy)_3^{2+}$ self-quenching in ZrPS. For example, self-quenching by triplet-triplet annihilation has been observed for $Ru(bpy)_3^{2+}$ in sodium dodecyl sulfate solutions.[40-42] Triplet-triplet annihilation can be ruled out as the self-quenching mechanism in the present case because single photon counting experiments use low light intensities. Therefore, the concentration of excited $Ru(bpy)_3^{2+}$ ($^*Ru(bpy)_3^{2+}$) is low and the probability of having two $^*Ru(bpy)_3^{2+}$ molecules close together is negligibly small.

An energy transfer mechanism for self-quenching can also be ruled out for $Ru(bpy)_3^{2+}$ because this mechanism would always leave an excited state $Ru(bpy)_3^{2+}$, i.e.

$$^*Ru(bpy)_3^{2+} + Ru(bpy)_3^{2+} \rightarrow Ru(bpy)_3^{2+} + {}^*Ru(bpy)_3^{2+} \qquad (8)$$

Reductive and oxidative quenching of excited state $Ru(bpy)_3^{2+}$ by ground state $Ru(bpy)_3^{2+}$ can be ruled out because these reactions are thermodynamically unfavorable (ΔE° = - 0.41 and - 0.44 V, respectively).

Our results, and those of Milosavljevic and Thomas, suggest that self-quenching of $Ru(bpy)_3^{2+}$ in ZrPS and cellulose occurs, upon diffusional collision, by catalyzed deactivation of the excited state. The deactivation occurs after diffusional collision of the two reactants. This collisional deactivation of the excited state is caused by an external spin-orbit coupling effect, which increases the probability for nonradiative decay.

The reaction mechanism is as follows

$$Ru(bpy)_3^{2+} + {}^*Ru(bpy)_3^{2+} \xrightarrow{k_q} 2Ru(bpy)_3^{2+} \qquad (9)$$

The probability of collisions during the $Ru(bpy)_3^{2+}$ excited state lifetime increases as the concentration of $Ru(bpy)_3^{2+}$ exchanged into ZrPS increases. We have previously reported[16] similar concentration effects which produce red shifts in the absorption and luminescence spectra of $Ru(bpy)_3^{2+}$ exchanged into ZrPS at high loading levels.

Assuming that the quenching reaction within ZrPS is diffusion controlled the self-quenching rate constant of 7.01 X 10^5 M^{-1} s^{-1} can be used to calculate the diffusion coefficient of $Ru(bpy)_3^{2+}$ in ZrPS via the Smoluchowski equation[43]

$$k_q = p4\pi RD'N/1000 \qquad (10)$$

where k_q is the quenching rate constant, p is the probability that a $Ru(bpy)_3^{2+}$-$^*Ru(bpy)_3^{2+}$ encounter will result in quenching, R is the sum of the ionic radii, D' is the sum of the diffusion coefficients of $Ru(bpy)_3^{2+}$(D^{2+}) and $^*Ru(bpy)_3^{2+}$(D^{*2+}), and N is Avogadro's number. Using Equation 10 and assuming that every encounter leads to quenching (p=1) we calculate a value for D' of 6.62 X 10^{-10} cm^2 s^{-1}. If we assume that the diffusion coefficients of $Ru(bpy)_3^{2+}$ and $^*Ru(bpy)_3^{2+}$ are the same then $D^{2+} = D^{*2+}$ = 3.31 X 10^{-10} cm^2 s^{-1}. This D value is an apparent diffusion

coefficient which includes contributions from physical diffusion and exciton exchange.

Bard et al. measured a diffusion coefficient of ca. 10^{-12} cm^2 s^{-1} for $Os(bpy)_3^{2+}$ and $Fe(bpy)_3^{2+}$ incorporated into montmorillonite clay.[44] Van Damme et al. report D values between 10^{-10} and 10^{-8} cm^2 s^{-1} for $Ru(bpy)_3^{2+}$ in extensively hydrated colloidal clay particles.[45] Thus, our D is in reasonable agreement with D's obtained for related systems. These D values are considerably smaller than the corresponding D's in water (ca. 10^{-6} cm^2 s^{-1}), and indicates slow diffusional movement of the $Ru(bpy)_3^{2+}$ ions through the interlayer space.

The diffusion coefficient may be used to calculate the root mean square (rms) distance travelled by $Ru(bpy)_3^{2+}$ during the excited state lifetime. This distance can be calculated from the Einstein-Smoluchowski equation[37]

$$R_t = (2Dt)^{1/2} \qquad (11)$$

where D is the diffusion coefficient and t is the lifetime of $^*Ru(bpy)_3^{2+}$. Equation 11 yields a R_t value of 2.3 Å for t = 806 ns. Therefore, during the lifetime of the excited state $Ru(bpy)_3^{2+}$ barely moves. The fact that dynamic quenching is observed indicates that when the probe ions are exchanged they occupy sites close to each other .

<u>MV^{2+} Quenching Studies.</u> Evidence for the mobility of ions through the interlayer space of ZrPS can also be obtained through

quenching studies. If all or part of the quenching mechanism is found to be dynamic, then the extent of diffusion of the ions through ZrPS can be determined. We decided to use methylviologen (MV^{2+}) as the quencher since the quenching reaction between $Ru(bpy)_3^{2+}$ and MV^{2+} in a variety of systems has been thoroughly studied. However, before the quenching reaction in ZrPS could be studied the interaction of MV^{2+} with ZrPS was investigated. We studied this interaction using X-ray diffraction experiments.

Figure 5 shows an X-ray powder diffraction pattern of a ZrPS sample that has been exchanged with MV^{2+}. The X-ray diffraction pattern reveals that the interlayer distance of ZrPS exchanged with MV^{2+} is 20.1 Å, an increase from the unexchanged ZrPS value of 16.1 Å.[18] The peak corresponding to the interlayer distance (d_{002}) is sharp, characteristic of a well ordered phase, with preferred orientation giving a well defined interlayer distance.

The increase in the ZrPS interlayer distance when MV^{2+} is exchanged suggests two possible orientations of MV^{2+} between the ZrPS layers. The first possible orientation can be deduced by considering the vertical distance available between the phenylphosphonate groups of ZrPS. A value of 13.5 Å can be calculated by subtracting the layer thickness of ZrPS, 6.6 Å for OPO_3ZrO_3PO-type layers,[18] from the interlayer distance of MV^{2+}-exchanged ZrPS, 20.1 Å. The length of MV^{2+}, calculated from the van der Waals radii of the constituent atoms, is 13.4 Å.[46] Therefore, MV^{2+} can adopt a vertical orientation perpendicular to the ZrPS layers.

The second possible orientation for the exchanged MV^{2+} can be deduced from the 4 Å increase in ZrPS interlayer distance when MV^{2+} is exchanged into ZrPS. The thickness of MV^{2+}, estimated to be 3.4 Å, or the thickness of the methyl groups in MV^{2+}, which is about 4 Å,[47] suggest that MV^{2+} can also adopt a completely flat, planar orientation. In this planar orientation MV^{2+} would be lying down between the sulfonated phenylphosphonate groups of ZrPS and would increase the interlayer distance by ca. 4 Å, precisely the value obtained experimentally (Figure 5). Similar orientations have been observed by Raupach et al.[46] and Knight and Denny[48], who observed that MV^{2+} adopts a planar conformation when incorporated into montmorillonite clay. Similarly, Szabo et al.[49] reported that strong binding of MV^{2+} in montmorillonite keeps the molecule in a planar conformation and leads to the observation of fluorescence from the incorporated MV^{2+}.

Probably, both MV^{2+} orientations (perpendicular and parallel) occur between the layers of ZrPS. Either of these orientations can permit diffusional movement of MV^{2+} through the ZrPS layers (see below). Finally, when both MV^{2+} and $Ru(bpy)_3^{2+}$ are exchanged into ZrPS the interlayer distance remains the same as that of MV^{2+}-exchanged ZrPS.

Figure 6 shows steady-state luminescence spectra of $Ru(bpy)_3^{2+}$ exchanged into ZrPS. Note that as the concentration of quencher is increased the emission intensity gets reduced indicating that MV^{2+} is quenching the $Ru(bpy)_3^{2+}$ emission. The quenching mechanism can not be elucidated from intensity data

alone; therefore, luminescence lifetime data for the quenching reaction were obtained.

Figure 7 shows typical $Ru(bpy)_3^{2+}$ luminescence decay curves at different concentrations of MV^{2+}. A static contribution to the quenching mechanism is obvious since the intensity at t=0 changes.[19,37] The reduction in the intensity at t=0 occurs because only probe molecules that are not statically quenched will emit.[19,37]

To elucidate the exact quenching mechanism we must fit the data to a quantitative decay model. This is a complicated task because there are both static and dynamic contributions to the quenching mechanism. We will begin by modeling only the dynamic part of the quenching process, by fitting the luminescence decay curves to two decay models. The two models are a monoexponential decay model and Albery's dispersed kinetics model. It will be seen that while both models fit the raw data, Albery's dispersed kinetics model gives a better fit and more reasonable results.

Figure 8 shows a typical fit to a monoexponential model (Equation 2).[50] Table III summarizes the lifetime, χ^2 and standard deviations obtained by fitting the data to a monoexponential model. The low χ^2 and standard deviation values indicate that the monoexponential decay model can be applied to these data. Fitting the decay curves to a biexponential decay model does not improve the fitting.

Figure 9 shows a typical fit of the Albery's dispersed kinetics model to the experimental luminescence decay data.

Table IV summarizes the lifetime, χ^2, and standard deviations obtained by fitting the data to the dispersed kinetics model. The χ^2 values at all the MV^{2+} concentrations are somewhat smaller for the dispersed kinetics model (Table IV) than for the monoexponential decay model (Table III); however, the standard deviations for the dispersed kinetics model are somewhat larger. Thus, it is difficult, based on statistical arguments, to chose one model over the other. However, as will be shown below, the dispersed kinetics model gives more reasonable results when we fit both the dynamic and static contributions of the quenching mechanism.

Figure 10 shows the Stern-Volmer plots obtained from the steady state data and the lifetime of maximum probability given by the fitting of each decay curve to Albery's Model. If quenching was purely dynamic (diffusional/collisional) both plots would be linear and they would be superimposable.[37] In the present case the curves are not colinear and the intensity data shows an upward curvature. These results are typical of a combination of dynamic and static quenching mechanisms.[37] The question now becomes what type of static quenching is occurring in this case.

The simplest type of static contribution is ground state complex formation. For a quenching mechanism with dynamic and static contributions via ground state complex formation, the Stern-Volmer equation becomes

$$I_o/I = (1 + K_d[MV^{2+}])(1 + K_s[MV^{2+}]) \qquad (12)$$

where K_d is the dynamic Stern-Volmer constant ($K_d = k_q \tau_o$) and K_s is the static Stern-Volmer constant (the equilibrium constant K_{eq} for complex formation). Equation 12 can be modified to allow graphical separation of K_s and K_d

$$I_o/I = 1 + (K_d + K_s)[MV^{2+}] + K_d K_s [MV^{2+}]^2 \qquad (13)$$

A plot of K_{app} ($K_{app} = (I_o/I - 1)/[MV^{2+}]$) vs. $[MV^{2+}]$ should give a straight line with slope equal to $K_d K_s$ and intercept equal to $K_d + K_s$.[19,37] If K_d is available from lifetime data, then K_s (or K_{eq}) can be evaluated from the intercept and the slope; the consistency of these two K_s values proves that the model is correct.[19]

Figure 11 shows a plot of K_{app} vs. $[MV^{2+}]$. In the present case we obtain from the lifetime data, a K_d value of 9.83 M^{-1}. The K_{eq} values calculated from the intercept and slope given by Equation 13 are 5.19 and 9.79 M^{-1}, respectively. The discrepancy in the two values indicates that static quenching by complex formation does not occur in the present case.

Although complex formation is ruled out, Figures 7 and 10 indicate that some type of nondiffusional quenching has to be operative in this system. Perrin proposed a model of static quenching which does not assumes complex formation.[51-53] The Perrin model proposes that at high quencher concentrations a fraction of the fluorophores are adjacent to a quencher at the moment of excitation, and thus immediately deactivated. This phenomenon is interpreted in terms of a "sphere of action" - a

volume of space that surrounds the excited state molecule. If a quencher molecule is within this quenching space, the probability of quenching is unity. The emitting probes are those for which there are no adjacent quencher within their "sphere of action".

For a situation with no diffusional contribution to the quenching mechanism the Perrin model proposes the following relationship

$$I_o/I = \exp([Q]VN/1000) = \exp([Q](4/3)\pi R_q N/1000) \qquad (14)$$

where V and R_q are the volume and radius of the sphere of action, respectively, and N is Avogadro's number. In the original formulation of the sphere of action model, R_q was defined as the sum of the radii of the reactants. However, it is important to point out that in the present case, the quenching reaction occurs via electron transfer. Electron transfer can occur over some distance, thus contact is not required. As a result, in electron transfer quenching reactions the radius of sphere of action is often larger than the sum of the radii of the reactants.

For a situation where quenching has diffusional and static components the Perrin model can be combined with the diffusional Stern-Volmer model. The modified form of the Stern-Volmer equation which describes the diffusional plus sphere of action model is[37]

$$I_o/I = (1 + K_d[Q]) \exp([Q]VN/1000) \qquad (15)$$

where V is the volume of the sphere, N is Avogadro's number and K_d is the dynamic quenching Stern-Volmer constant. The dynamic portion of the quenching can be isolated by dividing the raw I_o/I data by the variable exp([Q]VN/1000); this division by the exponential factor accounts for the proximity effect, and a linear Stern-Volmer plot should be obtained. This linear Stern-Volmer plot should be superimposable with the τ_o/τ Stern-Volmer plot obtained from lifetime measurements; if this is true this portion of the quenching is dynamic.[37]

Figure 12 shows the quenching data plotted in the form of the dynamic plus sphere of action model (Equation 15). The plot shows that the division of the I_o/I data by the exponential variable gives a curve colinear with the lifetime data; this colinearity means that the dynamic plus sphere of action model is correct. It is important to note that the only adjustable parameter used to fit this model is the volume of the "sphere of action". A sphere of action with a radius of 10.8 Å is obtained from the fit in Figure 12.

The 10.8 Å radius obtained from the data in Figure 12 is slightly larger that the sum of the geometric radii of $Ru(bpy)_3^{2+}$ and MV^{2+}, which is 10 Å.[54,55] The 10.8 Å radius is in excellent agreement with the literature value of 10.9 Å obtained by McLendon et al.[54] for the $Ru(bpy)_3^{2+}$-MV^{2+} system in rigid glycerol solution. Thus, the use of the Albery's dispersed kinetics model to analyze the lifetime data gives reasonable results for the quenching mechanism. In constrast, if the monoexponential decay

model is used, the analysis gives in an unreasonably large radius of the sphere of action of 12.8 Å. Therefore, the dispersed kinetics model gives a more reasonable result than the exponential model for the radius of the sphere of action. The dispersed kinetics model not only fits the experimental decay curves better that the monoexponential decay model, but it gives more reasonable results for the quenching mechanism. The dispersed kinetics model is then the preferred model for the analysis of the quenching luminescence transients in ZrPS.

From the diffusional component to the quenching mechanism we can calculate the diffusional bimolecular quenching rate constant k_q. The K_d value is 9.83 M^{-1} and the $Ru(bpy)_3^{2+}$ lifetime in ZrPS is 806 ns. The k_q value is calculated to be 1.2 x 10^7 M^{-1} s^{-1} ($k_q = K_d/\tau_o$). The k_q value obtained in ZrPS is smaller than the value obtained in water (3-5 X 10^8 M^{-1} s^{-1}),[36,56,57] but it is larger than the value obtained in the layered clay hectorite by Ghosh and Bard (k_q = 1.1 X 10^6 M^{-1} s^{-1}).[36] The smaller k_q value in ZrPS than in water indicates a slower movement of quencher ions through the interlayer space of ZrPS, which is also evident from the small D. The higher k_q value in ZrPS than in hectorite indicates that although the diffusion of ions in ZrPS is not very fast it is faster than in hectorite.

In their study of quenching in hectorite clay Ghosh and Bard[36] claimed that the low k_q value observed was due to segregation of the MV^{2+} and $Ru(bpy)_3^{2+}$ molecules in different clay layers. In hectorite clay the emission kinetics of adsorbed

$Ru(bpy)_3^{2+}$ in the presence of MV^{2+} were equal to the kinetics in the absence of MV^{2+}. In ZrPS the possibility of segregation is ruled out since our emission decay profiles are distinctively different in the presence and absence of MV^{2+}. The decay measurements prove that during the excited state lifetime the quencher ions interact with the probe molecules. No spatial separation due to segregation occurs in the ZrPS layers.

Assuming that the excited state reaction is diffusion controlled, the Smoluchowski equation (Equation 10) can be used, with the previously determined diffusion coefficient for $Ru(bpy)_3^{2+}$ in ZrPS, to calculate the diffusion coefficient for MV^{2+} in ZrPS; a D of 1.6×10^{-8} cm^2 s^{-1} is obtained. This D is two orders of magnitude larger than the D value for $Ru(bpy)_3^{2+}$ (3.3×10^{-10} cm^2 s^{-1}). Thus, the smaller MV^{2+} ion has higher mobility through the interlayer space of ZrPS than $Ru(bpy)_3^{2+}$.

The rms distance (R_t) travelled by MV^{2+} during the $Ru(bpy)_3^{2+}$ excited state lifetime can be calculated from the diffusion coefficient using Equation 11; a R_t of 16.6 Å is obtained. Compared to the R_t of $Ru(bpy)_3^{2+}$ (2.3 Å), the R_t of MV^{2+} indicates that during the lifetime of the excited state $Ru(bpy)_3^{2+}$ barely moves, whereas, MV^{2+} travels a longer distance.

The difference in mobilities between $Ru(bpy)_3^{2+}$ and MV^{2+} occurs because $Ru(bpy)_3^{2+}$ is a much bigger ion than MV^{2+}. $Ru(bpy)_3^{2+}$ (a spherical ion, 14 Å in diameter) can accommodate itself between the layers of ZrPS, but its movement is restricted by the protruding phenylphosphonate groups in the structure of

ZrPS. The space between the protruding phenylphosphonate groups is not big enough to facilitate diffusion of the $Ru(bpy)_3^{2+}$ ions. MV^{2+}, being a smaller ion (13.4 Å in length, 6.4 Å in width, 3.4-4 Å in thickness[46,47]), can tumble around, reptate, and diffuse more easily within this crowded microenvironment than $Ru(bpy)_3^{2+}$. The space between phenyl rings in ZrPS is big enough for MV^{2+} to move more easily through ZrPS than $Ru(bpy)_3^{2+}$. Therefore, the difference in size of the ions with respect to the structure of ZrPS governs their mobility.

CONCLUSIONS

The microenvironment within ZrPS restraints the movement of ions through the interlayer space, but diffusion leading to dynamic quenching reactions can occur. A model combining diffusional quenching and sphere of action quenching accounts for quenching of $Ru(bpy)_3^{2+}$ by MV^{2+} in ZrPS. These results provide another example of the rich variety of excited state reactions in heterogeneous systems. In the case of ZrPS the kinetics of the reactions reported here must be described by taking into account the heterogeneous nature of ZrPS.

New derivatives of α-ZrP similar in structure to ZrPS can be synthesized with increased distance between the phenyl rings. This bigger space should increase the mobility of ions through ZrPS. Furthermore, studies on layered systems with well defined separation between an excited probe molecule and a quencher can provide insights into the distance dependence of electron transfer. Studies of the distance dependence of electron

transfer reactions in such systems is an extremely interesting and active area of research. We are currently pursuing these efforts and hope to report our results in the near future.

ACKNOWLEDGEMENT. Financial support for this work was provided by the Robert A. Welch Foundation, the Office of Naval Research, and the Air Force Office of Scientific Research. We gratefully acknowledge partial support of this research by the Regents of Texas A&M University through the AUF-sponsored Materials Science and Engineering Program. J.L.C. acknowledges support from the Texas A&M University Minority Merit Fellowship.

References

(1) Connolly, J. S. Photochemical Conversion and Storage of Solar Energy; Academic: New York, 1981.

(2) Energy Resources Through Photochemistry and Catalysis; Grätzel, M., Ed.; Academic: New York, 1983.

(3) Proceedings of the 6th International Conference on Photochemical Conversion and Storage of Solar Energy; Nouv. J. Chem. 1987, 11, 79-207.

(4) Inorganic Ion Exchange Materials; Clearfield, A., Ed.; CRC: Boca Raton, FL, 1982.

(5) Alberti, G. Acc. Chem. Res. 1978, 11, 163.

(6) Intercalation Chemistry; Whittingham, M. S.; Jacobson, A. J., Eds.; Academic: New York, 1982.

(7) Clearfield, A. Chem. Rev. 1988, 88, 125.

(8) Alberti, G.; Constantino, U.; Allulli, S.; Tomassini, N. J. Inorg. Nucl. Chem. 1978, 40, 1113.

(9) Dines, M. B.; DiGiacomo, P. M. Inorg. Chem. 1981, 20, 92.

(10) Dines, M. B.; DiGiacomo, P. M.; Callahan, K. P.; Griffith, P. C.; Lane, R. H.; Cooksey, R. E. In Chemically Modified Surfaces in Catalysis and Electrocatalysis; Miller, J. S., Ed.; ACS Symposium Series 192; American Chemical Society: Washington, DC, 1982; pp 223-240.

(11) DiGiacomo, P. M.; Dines, M. B. Polyhedron 1982, 1, 61.

(12) Alberti, G.; Constantino, U. J. Mol. Catal. 1984, 27, 235.

(13) Ferragina, C.; La Ginestra, A.; Massucci, M. A.; Patrono, P.; Tomlinson, A. A. G. J. Phys. Chem. 1985, 89, 4762.

(14) Alberti, G. In Recent Developments in Ion Exchange; Williams, P. A., Hudson, M. J., Eds.; Elsevier Applied Science: London, 1987, pp 233-248.

(15) Alberti, G.; Constantino, U.; Marmottini, F. In Recent Developments in Ion Exchange; Williams, P. A., Hudson, M. J., Eds.; Elsevier Applied Science: London, 1987, pp 249-256.

(16) Colón, J. L.; Yang, C.-Y.; Clearfield, A.; Martin, C. R. J. Phys. Chem. 1988, 92, 5777.

(17) Albery, W. J.; Barlett, P. N.; Wilde, C. P.; Darwent, J. R. J. Am. Chem. Soc. 1985, 107, 1854.

(18) Yang, C.-Y.; Clearfield, A. React. Polym., Ion Exch., Sorbents 1987, 5, 13.

(19) Demas, J. N. Excited State Lifetime Measurements; Academic: New York, 1983.

(20) O'Connor, D. V., Phillips, D. Time Correlated Single Photon Counting; Academic: London, 1984.

(21) Bevington, P. R. Data Reduction and Error Analysis in the Physical Sciences; McGraw Hill: New York, 1969.

(22) James, D. R.; Ware, W. R. Chem. Phys. Lett. 1985, 120, 450.

(23) James, D. R.; Ware, W. R. Chem Phys. Lett. 1986, 126, 7.

(24) James. D. R.; Turnbull, J. R.; Wagner, B. D.; Ware, W. R.; Petersen, N. O. Biochemistry 1987, 26, 6272.

(25) Siemiarczuk, A.; Ware, W. R. J. Phys. Chem. 1987, 91, 3677.

(26) Lakowicz, J. R.; Cherek, H.; Gryczynski, I.; Joshi, N.; Johnson, M. L. Biophys. Chem. 1987, 28, 35.

(27) Lakowicz, J. R.; Johnson, M. L.; Wiczk, W.; Bhat, A.; Steiner, R. F. Chem. Phys. Lett. 1987, 138, 587.

(28) Gryczynski, I.; Wiczk, W.; Johnson, M. L.; Lakowicz, J. R. Chem. Phys. Lett. 1988, 145, 439.

(29) Alcala, J. R.; Gratton, E.; Prendergast, F. G. Biophys. J. 1987, 51, 587.

(30) Alcala, J. R.; Gratton, E.; Prendergast, F. G. Biophys. J. 1987, 51, 597.

(31) Alcala, J. R.; Gratton, E.; Prendergast, F. G. Biophys. J. 1987, 51, 925.

(32) Parasassi, T.; Conti, F.; Gratton, E.; Sapora, O. Biochim. Biophys. Acta 1987, 898, 196.

(33) Colón, J. L.; Martin, C. R. submitted for publication in J. Phys. Chem.

(34) Turro, N. J.; Kumar, C. V.; Grauer, Z.; Barton, J. K. Langmuir 1987, 3, 1056.

(35) Webster's II New Riverside University Dictionary; The Riverside Publishing Company: Boston, 1984.

(36) Ghosh, P. K.; Bard, A. J. J. Phys. Chem. 1984, 88, 5519.

(37) Lakowicz, J. R. Principles of Fluorescence Spectroscopy; Plenum: New York, 1983.

(38) Stern, O.; Volmer, M. Z. Phys. 1919, 20, 183.

(39) Milosavljevic, B. H.; Thomas, J. K. J. Phys. Chem. 1983, 87, 616.

(40) Lachish, U.; Ottolenghi, M.; Rabani, J. J. Am. Chem. Soc. 1977, 99, 8062.

(41) Baxendale, J. H.; Rodgers, M. A. J. Chem. Phys. Lett. 1980, 72, 424.

(42) Baxendale, J. H.; Rodgers, M. A. J. J. Phys. Chem. 1982, 86, 4906.

(43) Smoluchowski, M. V. Z. Phys. Chem. 1917, 92, 129.

(44) Ege, D.; Ghosh, P. K.; White, J. R.; Equey, J.-F.; Bard, A. J. J. Am. Chem. Soc. 1985, 107, 5644.

(45) Habti, A.; Keravis, D.; Levitz, P.; Van Damme, H. J. Chem. Soc., Faraday Trans 2 1984, 80, 67.

(46) Raupach, M.; Emerson, W. W.; Slade, P. G.; J. Colloid Interface Sci. 1979, 69, 398.

(47) Summers, L. A. The Bipyridinium Herbicides; Academic: New York, 1980.

(48) Knight, B. A. G.; Denny, P. T. Weed Res. 1970, 10, 40.

(49) Villemure, G.; Detellier, C.; Szabo, A. G. J. Am. Chem. Soc. 1986, 108, 4658.

(50) The logarithmic plot shows some nonlinearity; this nonlinearity is caused by the noise background signal. The fitting algorithms add a parameter that accounts for this background.

(51) Perrin, F. C. R. Acad. Sci., Paris 1924, 178, 1978.

(52) Perrin, F. Ann. Chem. Phys. 1932, 17, 283.

(53) Turro, N. J. Modern Molecular Photochemistry; Benjamin/Cummings: Menlo Park, CA, 1978.

(54) Guarr, T.; McGuire, M.; Strauch, S.; McLendon, G. J. Am. Chem. Soc. 1983, 105, 616.

(55) Stradowski, Cz.; Wolszczak, M. In Photochemistry and Photophysics of Coordination Compounds; Yersin, H.; Vogler, A., Eds.; Springer-Verlag: Berlin, 1987; pp 125-128.

(56) Grätzel, M.; Kiwi, J.; Kalyanasundaram, K. Helv. Chim. Acta 1978, 61, 2720.

(57) Darwent, J. R.; Kalyanasundaram, K. J. Chem. Soc., Faraday Trans. 2 1981, 77, 373.

Table I. Kinetic and Statistical Parameters Obtained by Fitting a Biexponential Decay Model to the Experimental $Ru(bpy)_3^{2+}$ Emission Data in ZrPS.

$Ru(bpy)_3^{2+}$, [a] %	τ_{short}(%), [b] ns	τ_{long}(%), [b] ns	χ^2 [c]
2.2	243 ± 65 (15.62)	1,100 ± 88 (84.38)	2.20
8.0	300 ± 58 (13.85)	1,053 ± 60 (86.15)	2.36
21.0	277 ± 58 (12.77)	904 ± 44 (87.23)	2.38
42.8	198 ± 23 (11.43)	717 ± 18 (88.57)	2.40
52	173 ± 15 (10.69)	666 ± 13 (89.31)	2.48

[a] Percent of $-SO_3^-$ sites in ZrPS occupied by $Ru(bpy)_3^{2+}$.

[b] Error in lifetime value given as one standard deviation. Value in parenthesis is the percent of that lifetime component to the total luminescence decay.

[c] Reduced chi square value (see Equation 1).

Table II. Kinetic and Statistical Parameters Obtained by Fitting the Dispersed Kinetics Model to the Experimental $Ru(bpy)_3^{2+}$ Emission Data in ZrPS.

$Ru(bpy)_3^{2+}$, % [a]	$\bar{k}$ X 10^6, s^{-1}	τ, ns [b]	γ	χ^2 [c]
2.2	1.241	806 ± 34	0.83	1.68
8.0	1.445	692 ± 9	1.04	2.38
21.0	1.526	655 ± 9	1.01	2.37
42.8	1.950	513 ± 4	1.07	2.42
52	2.102	478 ± 3	1.14	2.52

[a] Percent of $-SO_3^-$ sites in ZrPS occupied by $Ru(bpy)_3^{2+}$.

[b] Error in lifetime value given as one standard deviation.

[c] Reduced chi square value (see Equation 1).

Table III. Kinetic and Statistical Parameters Obtained by Fitting a Monoexponential Decay Model to the Experimental $Ru(bpy)_3^{2+}$ Emission Quenching Data in ZrPS.

$[MV^{2+}]$,M	τ, ns [a]	χ^2 [b]
0.00	710 ± 12	1.78
0.02	674 ± 10	1.31
0.14	493 ± 9	1.52
0.47	329 ± 12	1.46

[a] Error in lifetime value given as one standard deviation.

[b] Reduced chi square value (see Equation 1).

Table IV. Kinetic and Statistical Parameters Obtained by Fitting a Dispersed Kinetics Decay Model to the Experimental $Ru(bpy)_3^{2+}$ Emission Quenching Data in ZrPS.

$[MV^{2+}]$,M	$\bar{k}$ X 10^6, s^{-1}	τ, ns [b]	γ	χ^2 [a]
0.00	1.241	806 ± 34	0.83	1.68
0.02	1.289	776 ± 30	0.95	1.24
0.14	1.917	522 ± 20	1.65	1.16
0.47	6.838	146 ± 14	2.42	1.02

[a] Error in lifetime value given as one standard deviation.

[b] Reduced chi square value (see Equation 1).

Figure 1. Typical luminescence decay curves for $Ru(bpy)_3^{2+}$-exchanged ZrPS. Loading levels (percent of sulfonate sites associated with $Ru(bpy)_3^{2+}$) are: 1 - 2.2%, 2 - 21%, 3 - 42%, 4 - 52%.

Figure 2. Decay model fits to an experimental decay curve for a 43% $Ru(bpy)_3^{2+}$-exchanged ZrPS. (A) Dispersed kinetics model fit; (B) Biexponential decay model fit. The points are the experimental curves and the lines the calculated curves.

Figure 3. Mean $Ru(bpy)_3^{2+}$ luminescence lifetime at various loading levels in ZrPS.

Figure 4. Rate constants for $Ru(bpy)_3^{2+}$ luminescence decay vs. concentration of $Ru(bpy)_3^{2+}$ in ZrPS.

Figure 5. X-ray diffraction pattern of MV^{2+}-exchanged ZrPS.

Figure 6. Steady state luminescence spectra for the quenching of $Ru(bpy)_3^{2+}$ with MV^{2+} in ZrPS. The percent of sulfonate sites associated with MV^{2+} are given in the curves.as follow: A, 0%; B, 1%; C, 6%; D, 20%.

Figure 7. Typical luminescence decay curves for $Ru(bpy)_3^{2+}$-exchanged ZrPS at various loading levels of MV^{2+}. Loading levels (percent of sulfonate sites associated with MV^{2+}) are: 1 - 0%; 2 - 1%; 3 - 6%; 4 - 20%.

Figure 8. Typical monoexponential decay model fit to the $Ru(bpy)_3^{2+}$ luminescence quenching with MV^{2+} in ZrPS. Points-experimental data, solid curve-best fit to a monoexponential decay model (see reference 50).

Figure 9. Typical dispersed kinetics model fit to the $Ru(bpy)_3^{2+}$ quenching with MV^{2+} in ZrPS (with 1% of MV^{2+} exchanged). The points are the experimental curve and the line the calculated curve using the dispersed kinetics model.

Figure 10. Stern-Volmer plot for the quenching of $Ru(bpy)_3^{2+}$ by MV^{2+} in ZrPS obtained with the dispersed kinetics model fit to the transient data.

Figure 11. Dynamic plus static model fit to the quenching data(K_{app} vs. $[MV^{2+}]$. Dynamic data obtained from the dispersed kinetics model fit to the transient data.

Figure 12. Sphere of action fit to the steady-state emission quenching data (assuming dispersed kinetics) in ZrPS. V is the volume of the sphere of action, and N' is 6.02×10^{20}.

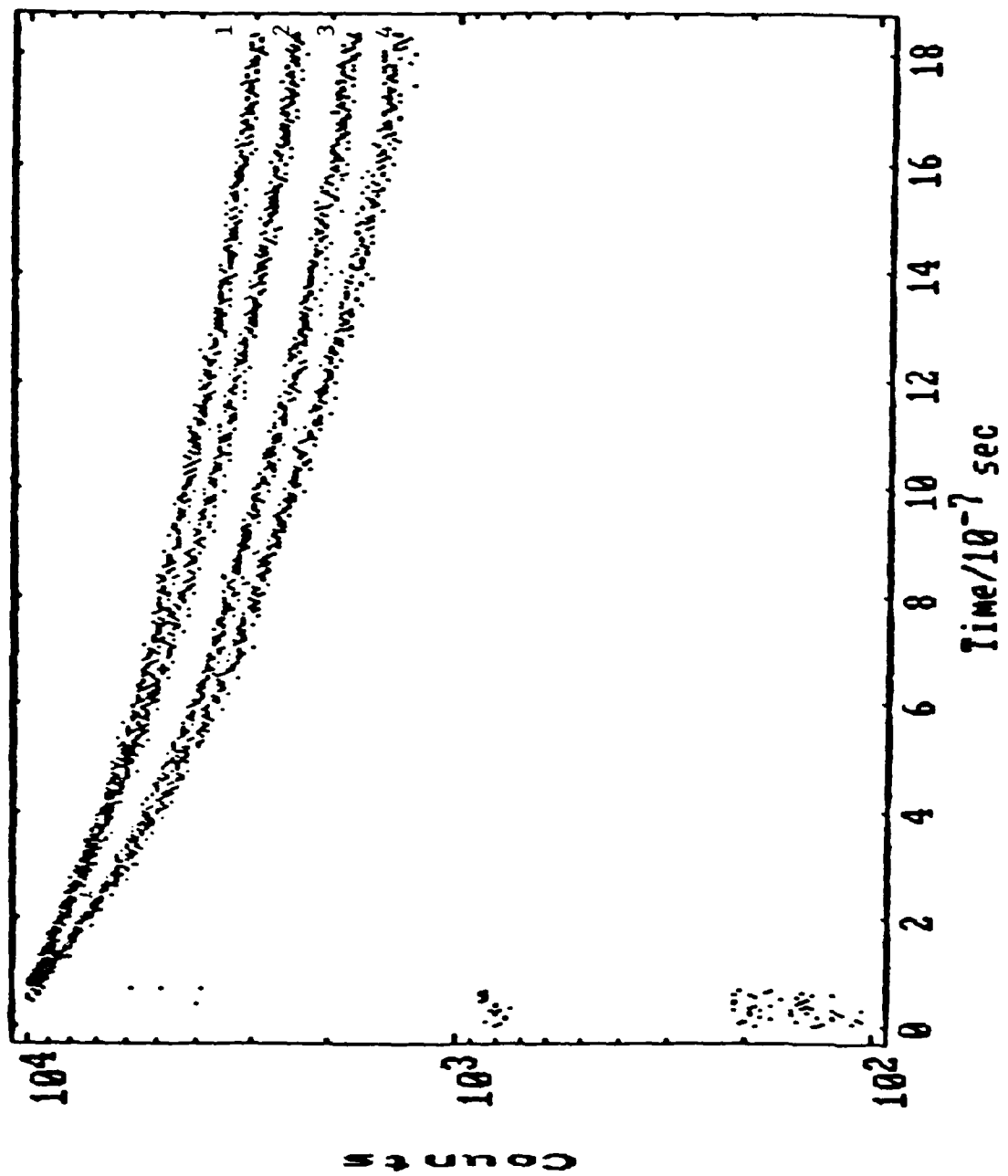

Fig. 1